Chapter 6

Coupled confocal microscopes with polarization-selective outputs and fiber access in a cryogenic system

Abstract

This chapter presents the design and performance analysis of instrumentation that allows for optically accessing a small measurement volume with two uniaxial confocal microscopes in series. For application in a helium bath cryostat, it can be accessed with three fibers: one single-mode polarization-maintaining fiber as input, and two multi-mode fibers as outputs that are connected to collect two orthogonal linear polarizations of light. The polarization filtering is realized with a compact wire-grid polarizer inside the output microscope. The unit is made to fit in the bore of a superconducting magnet of 5 cm diameter, and aligned for measuring in Voigt geometry. This setup is designed for quantum-optical experiments with donor-bound electrons in GaAs, and optimized for wavelengths around 820 nm. Preliminary spectroscopic experiments on a thin layer of n-GaAs material are presented as examples that can assess the performance of the setup.

6.1 Introduction

Building on the instrumentation development that was reported in Chapter 5, we present here further development of a cryogenic microscope system for the research project of this thesis. The key innovation is that a second confocal microscope was added, in a uniaxial manner, that allows for coupling light out of the measurement volume and cryostat for further processing on an optical table in our laboratory (all the work presented up to this point had a photodetector in the cryogenic measurement volume). While the incoming fiber used remained a single-mode polarization-maintaining fiber, for the output two large-core multi-mode fibers were used, since using a single-mode fiber as well would give extremely challenging alignment and stability issues. To still maintain clear polarization information for the outcoming light, a wire-grid polarizer is placed in the measurement volume, for steering two orthogonal linear polarizations into the two different multi-mode fibers. This instrumentation has not been used for the results presented in the previous chapters, but has been essential for new experimental studies by our team on the GaAs D^0 system [1, 2, 3]. In the remainder of this chapter we first focus on design and construction aspects, before presenting results of testing the instrument performance.

6.2 Three-fiber coupled confocal microscopes: design and construction

Figure 6.1 presents a schematic overview of the three-fiber coupled confocal microscope system. It is a compact instrument where two microscopes are aligned along one axis. Light of two orthogonal linear polarizations can be fed into (or collected, see Chapter 5) the measurement volume, as carried by a polarization-maintaining fiber. In the sample space these polarizations are identified with respect to the direction of the applied magnetic field: H-polarization (orthogonal to field) and V-polarization (parallel to field). For the ability to analyze (or do other further processing) signal fields that have been transmitted through a material in the sample volume, a second microscope, coupled to a pair of large-core fibers, is added along the optical path. These efficiently-coupled (for collecting light) large-core fibers also facilitate highly-efficient detection of luminescence signals from the sample volume. The output confocal microscope is axially aligned to the light propagation direction of the input confocal microscope, and has lenses that have about a factor four larger diameter lenses as compared to the input

microscope (see Chapter 5). The unit is mounted in a small vacuum chamber (dipstick approach) that fits in the bore of a superconducting magnet (5 cm diameter), in a cryogenic helium-bath environment (but it can in principle be used at any temperature that is created around the vacuum chamber). The alignment of the optical path in the measurement volume corresponds to measuring in Voigt geometry.

The design accounts for the technological challenge to have a setup that can sustain the temperature of liquid helium, while it remains compatible with an (only) three-axis control and feedback mechanism for placing a sample in the focus of the input microscope (see Chapter 5). Notably, this function should be robust against thermal displacements of parts of microscopes over tens of micrometers when the temperature is changed from 300 K to 4.2 K. Further, also this system should be compatible with applying magnetic fields up to about 10 T. The coupled microscopes are designed in such a way that –if required– they can be easily disassembled and reassembled. To minimize stray reflections the overall structure and lens mounts are made of Vespel, a type of plastic developed for space technology. This also avails easy engineering and a way to fix the optical parts with minimum risk of damaging them. The optical parts are selected for using them at wavelengths near 820 nm, which is optimal for spectroscopic studies of the D^0 system in GaAs.

6.2.1 Input part, sample space and sample holder

To send polarized light in, we use a PANDA-type polarization-maintaining single-mode fiber with a numerical aperture (NA) of 0.13 and a core diameter of 5 μm. This fiber has different refractive indices for H- and V-polarization and maintains the propagating polarizations in a locked manner, even in strong magnetic fields. The polarization is tested to be maintained up to 9 T [4, 5]. It circumvents the need for building a (bulky) setup for polarization purification inside the dipstick. The light propagation direction out of the polarization-maintaining fiber (Fig. 6.1) is altered by 90° using a prism mirror (part Thorlabs MRA05-E02) to give Voigt geometry in the sample volume. The light coming out of the fiber has a divergent output. This beam is collimated with an aspheric lens of 1.5 mm clear aperture, and 5 mm focal distance and a NA of 0.15 (part Thorlabs 350430). The light is focused in the sample volume with another aspheric lens with focus at 1.45 mm and a NA of 0.55 (part Thorlabs 350140).

The sample space is after the input microscope and is available for use over

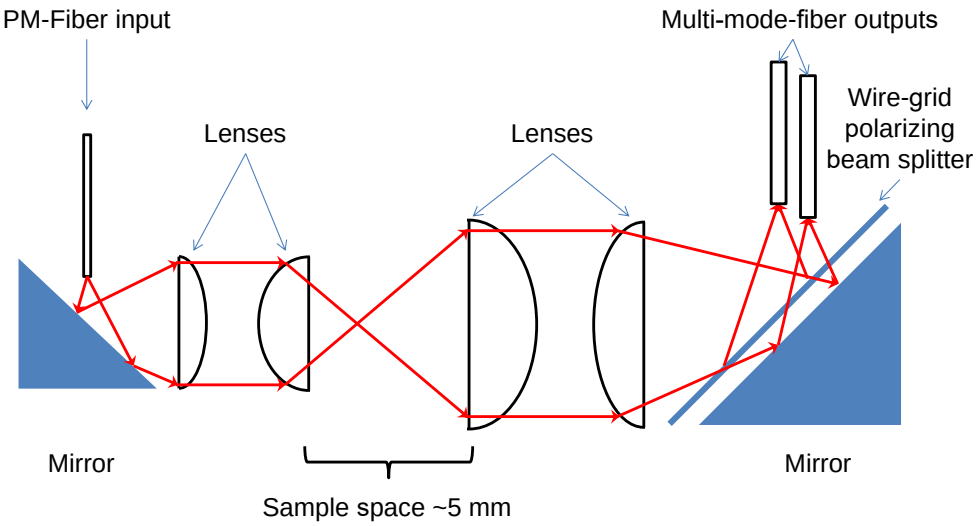

Figure 6.1: Schematic representation of the coupled confocal microscope setup. The single-mode polarization-maintaining fiber (PM Fiber), mirror, and a set of two aspheric lenses, form the input part of the setup. It is followed by the sample space, which contains the overlapping focus of the incoming and outgoing optical paths. The sample space along the optical path is about 5 mm. Samples are placed on a copper cold finger which is attached to a three-axes (xyz) piezo-motor control stage for controlling the the sample position with respect to the focus. The next pair of aspheric lenses form a second confocal microscope which has a wire-grid polarizer in the optical path according to two linear orthogonal polarizations, which each couple into one of two multi-mode fibers that carry light out of the dipstick.

a distance of about 5 mm along the optical path (Fig. 6.1). For our studies on n-GaAs, we typically adhere thin n-GaAs layers on a sapphire substrate. In turn, the sapphire is mounted on a narrow copper cold finger using silver paint. The copper cold finger is attached to a piezo-motor control stage (part Attocube ANC120) for precise control in x-, y- and z-direction.

6.2.2 Output part

Along the optical path, after the sample volume, light is collected and collimated using an aspheric lens with a clear aperture of 4.95 mm, focal distance of 4.51 mm, and a NA of 0.55 (Fig. 6.1). The second lens of the output microscope is an aspheric lens with a focal distance of 13.86 mm and clear aperture of 5.1 mm. This lens focusses the collimated light on the end facets of multi-mode fibers with

a core of 1000 μm diameter (part OZ Optics VAC-01-V-QMMJ-3, XF-IRVIS-1000/1100-3- 6.6, 1.4:AR2).

For separating this output according to linear H- and V-polarizations, a wire-grid polarizing beam splitter (WGP) (part Edmund Optics #48-544), made of silver wires on a 700 μm-thick Corning glass plate (type 1737F, refractive index $\sim$1.51) is placed in the converging output path of the microscope, before the fiber entries. This WGP provides a selective reflectivity and transmission for the H- and V-polarized light. Before we placed the WGP inside the output microscope we carried out an experimental analysis of the reflection and transmission of this system for defining the optimal orientation of the WGP. The WGP is coated on one side with anti-reflection coating for wavelengths between 420 and 670 nm, for minimizing the Fabry-Pérot effect in the glass layer. This means that at our operating wavelengths of $\sim$820 nm, a weak Fabry-Pérot effect is expected, since we use the WGP outside the specified application range (a better model was not available). The results from the above considerations match well with the observations of the polarization filtering by WGP. Hence, we decided to place WGP in such a way that H- (in WGP documentation S-)polarized light will be reflected from the front side (with the wires) of the WGP and V- (in WGP documentation P-)polarized light will be transmitted through the WGP surface.

This results in the following design for light that travels out of the sample volume to the WGP. The part with H-polarized light is reflected from the surface of the WGP and is collected in the first multi-mode fiber. The V-polarized part of the light, which is transmitted through WGP, gets reflected from a mirror (part Thorlabs MRA05-E02) and passes again through the same WGP, before it comes to its focus at the entry of the second multi-mode fiber.

6.3 Performance tests

For testing this system's performance we carried out several experiments with or without an n-GaAs layer in the system, and both for the system at room temperature and 4.2 K. It includes checks of the output stability as a function of time, as a function of wavelength, and test of the polarization separation in the two output channels. Further, we used this system for performing transmission and photoluminescence spectroscopy on a thin n-GaAs layer. We used here again GaAs layers of 10 μm thickness, with Si doping at $\sim 3 \times 10^{13}$ cm^{-3} (for details see Chapters 2, 3).

6.3.1 Two-channel output stability

The stability of coupling light into the output channels is important for sensitive quantum-optical experiments to be performed in the future. The output stability for the system at 4.2 K was monitored as a function of time for both the output channels, such that it also recorded cross talk between the two output channels. For this test there was no GaAs sample in the optical path. The results are presented in Fig. 6.2. These signals are normalized to a reference signal from the laser to remove the influence of drifts in laser power. For these results, either H-polarized light or V-polarized light was sent into the setup via the single-mode fiber, while the optical powers coming out of the H- and V-polarization output channels were monitored.

For both input polarizations the strongest output signal appears in the corresponding channel (for this check the desired transfer H to H and V to V). However, for both cases there also appears significant output in the other channel (H to V, and V to H), on the order of 50% of the desired signal. For a small part ($\sim$5%) this is due to imperfect alignment of the polarization orientation as it enters the measurement volume. However, it also shows that at 4.2 K thermal contractions (possibly giving alignment distortions) reduce the WGP performance to levels that are far from ideal. Nevertheless, with this degree of polarization-selective output one can still analyze the polarization of signal from the measurement volume (below, Ref. [1]). Concerning the stability in time, these transfer properties show slow drifts of a few percent, which we consider satisfactory.

Results of a second test that we performed are presented in Fig. 6.3 (system again at 4.2 K, no GaAs material in the optical path). The goal of this test was to investigate the variation of coupling efficiencies into the output channels as as a function of wavelength. There is indeed such a dependence, which appears in the form of a weak Fabry-Pérot modulation. It occurs both for the H- and V-polarized case, with opposite phase. Since the WGP has clearly non-ideal behavior (see above), this can indeed be expected. The weak Fabry-Pérot effects then occur for both reflection on, and transmission trough the glass plate of the WGP.

6.3.2 Transfer losses and two-channel polarization analysis

As an extension of the above tests, we performed a study that compared the performance at room temperature and 4.2 K. Further, we more precisely follow

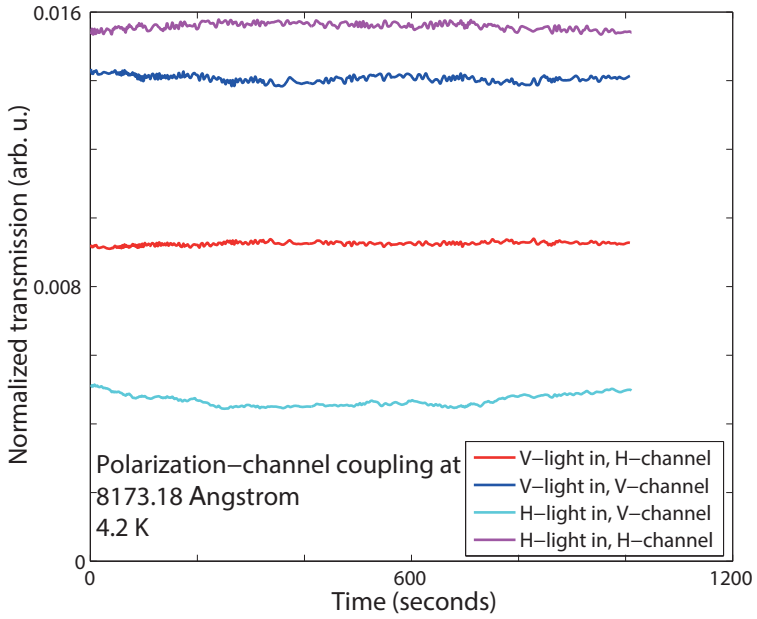

Figure 6.2: The output stability of the H- and V-polarization channels as a function of time. H-polarized light was sent into the setup and detected for the two outputs. For this case, the desired output (H-channel) is measured (purple trace), while the undesired cross-talk into the V-channel is measured as well (light-blue trace). For similar measurements carried out with sending V-polarized light into the system, the V-polarized channel output is presented with the dark-blue trace, and the H-channel output is presented with the red trace.

the normalized power transfer of laser beams entering and leaving the system, and better measure the behavior of the two-channel power distribution by the WGP as a function of polarization.

For these tests we fixed the input wavelength, and determined the power output of the H- and V-channel, each normalized to the laser power sent into the polarization-maintaining fiber. As a first step (at room temperature and with the measurement volume open), we confirmed the proper alignment of the H- and V-axis of the polarization-maintaining-fiber connection (the output) at the entry of the measurement volume. In addition, we marked the rotation settings of a half-wave plate that was placed right before the entry of this polarization-maintaining fiber that give pure H- and V-polarization in the sample space inside the microscope (before this half-wave plate we purified the beam to a linear polarization at the level of 10^5 to 1). These angles were 238° for V-polarization, and 328° for H-polarization (measured with respect to an arbitrary reference point

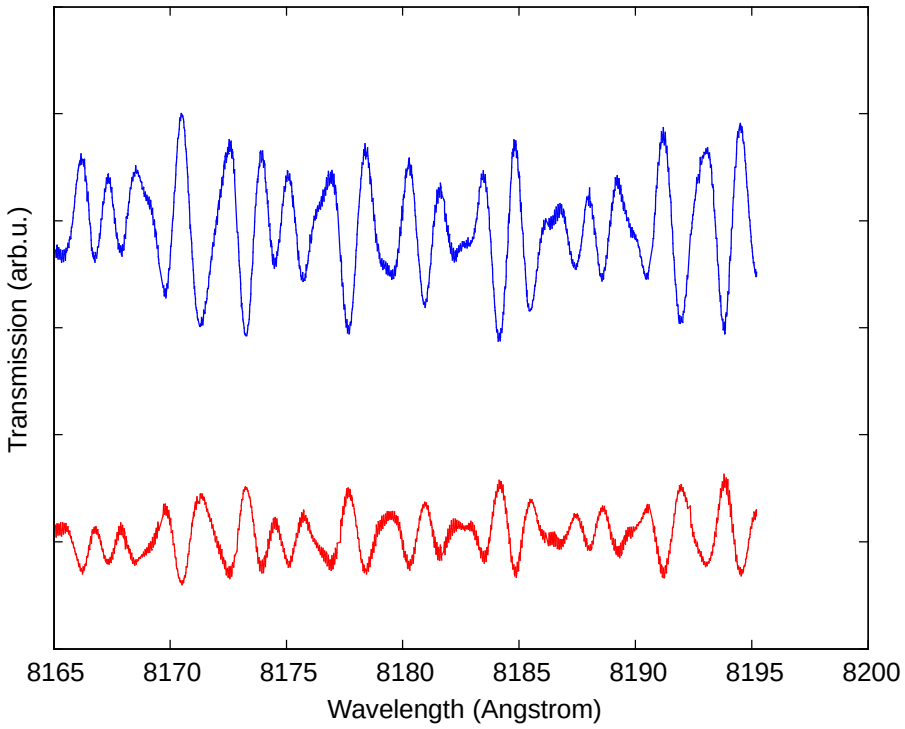

Figure 6.3: The output of the H- and V-polarization channels as a function of input wavelength, measured with input polarization aligned to the relevant output channel. The measured output signals show weak out-of-phase Fabry-Pérot oscillations.

in the mechanical mount), and are marked as vertical black lines (separated by 90°) in Fig, 6.4.

In turn, with the full system assembled, we studied the powers coming out of the H- and V-channel output fibers as a function of the rotation of the half-wave plate. Figure 6.4(a) presents the results of this test (with sinusoidal fits to the measured dependence on angle). Qualitatively, these two output signals show the expected sinusoidal behavior with opposite phase. The angles of the half-wave-plate rotation that lead to maximum power in the H- or V-channel are close to the expected setting: there is a $\sim 4^\circ$ offset, which is compatible with the precision of mounting that could be achieved for the polarization-maintaining fiber. Further, the measured power levels confirm a power loss of only a few percent, compatible with the performance of the anti-reflection coatings at all parts.

Figure 6.4(b) presents the results of performing the same measurements after cooling the system to 4.2 K. The outcome of these experiments was similar, but there are two significant differences. The power transfer through the entire system

decreased by about a factor 10, and the rotation offset between controlling pure H- and V-polarization and the observed maximum powers in the H- and V-output channels changed from ∼4° to ∼14° in the opposite direction. This indicates that the thermal contractions of the system indeed lead to a significant alignment disturbance. The behavior of the system on this aspect can probably be improved by designing a mechanical construction (Fig. 6.1) that is fully symmetric around the optical axis.

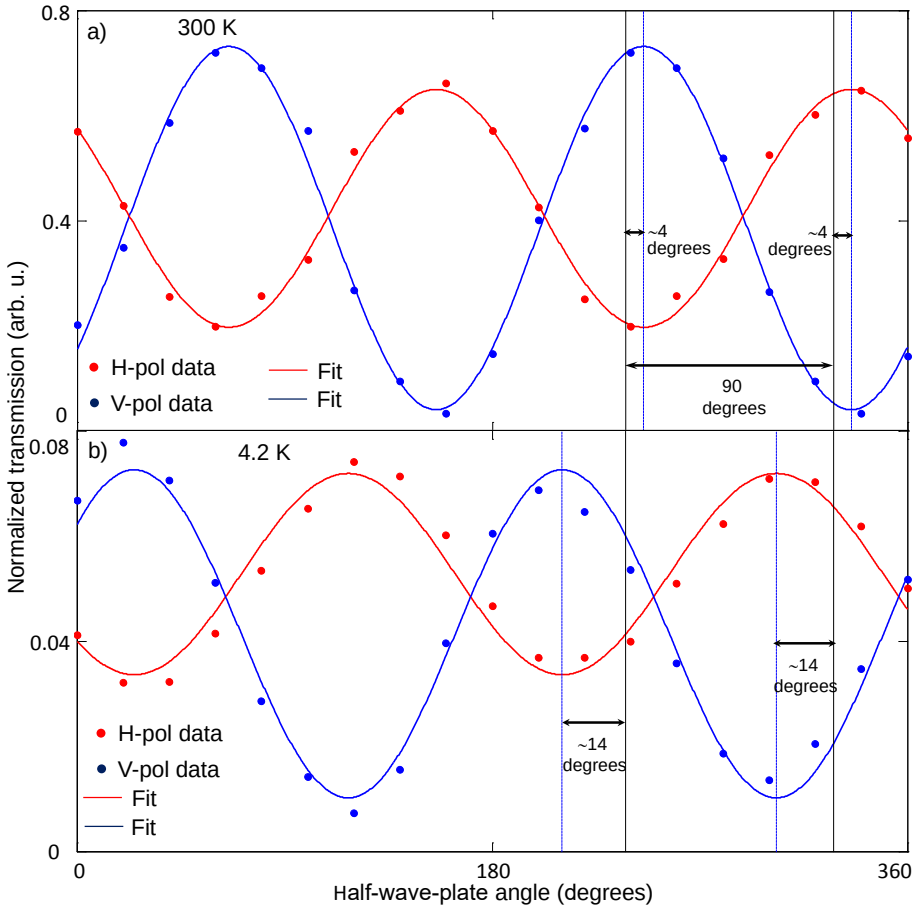

Figure 6.4: Results from testing polarization separation into the H- and V-polarization output channels, obtained with the system at room temperature **(a)** and 4.2 K **(b)**. The measured results (dots) represent normalized intensity output from the two different multi-mode-fiber output channels (as labeled) as a function of input polarization (controlled with a half-wave plate before the input of the polarization-maintaining fiber at room temperature). The solid traces are the result of fitting a sinusoidal dependence on the measurement results.

6.3.3 Spectroscopy tests on n-GaAs

Further performance tests were carried out by executing measurements on the n-GaAs layer. We first present transmission and photoluminescence spectroscopy results, before presenting tests of using the setup as an imaging tool.

Transmission spectroscopy

Figure 6.5(a) presents results from a single-laser-scan transmission spectroscopy study on the n-GaAs layer (see also Chapter 3). Here the detector measured light collected via the V-channel output. The material was at 4.2 K and in zero magnetic field. The results demonstrate that detection of transmitted light gives spectroscopy results that are in quality at least similar to the results in Fig. 3.2. The spectrum shows again the typical features for low-doped n-GaAs (absorption from free-exciton $X_{n=1}$ transitions, and D^0-D^0X transitions).

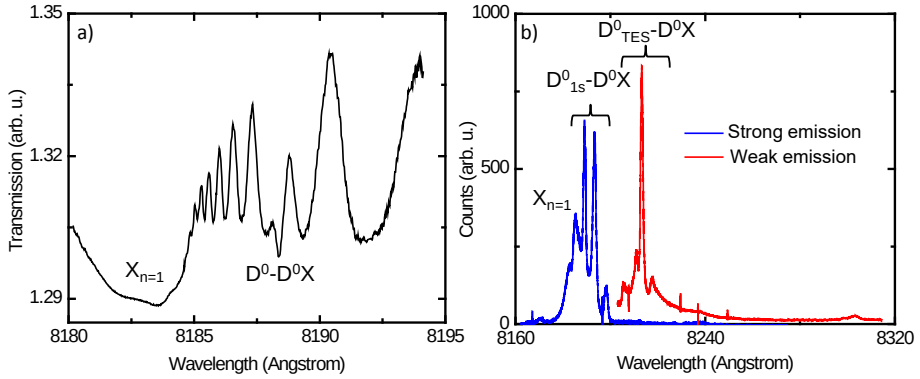

Figure 6.5: (a) Transmission spectrum for the n-GaAs layer at 0 T field. The observed transitions are identified and labeled as D^0-D^0X transitions, and the free-exciton $X_{n=1}$ transition. **(b)** Photoluminescence spectrum from the n-GaAs layer. The observed spectral lines are identified and labeled as emission from $X_{n=1}$ free-exciton transitions, several lines of D^0_{1s}-D^0X transitions, and several lines of D^0_{TES}-D^0X transitions (see main text). These spectra were detected via the channel that collects V-polarized light. The red trace (for weaker emission) was obtained by spectral blocking of the stronger emission (peaks in the blue trace), and using a 100 times longer integration time for the CCD camera.

Photoluminescence spectroscopy

Figure 6.5(b) presents results that demonstrate the use of the new output channels for collecting photoluminescence (PL) signals from the n-GaAs layer. The results were obtained with the sample at 4.2 K, and in zero magnetic field.

The sample was illuminated via the polarization-maintaining fiber, with a laser tuned to a photon energy higher than the band gap (blocked from the spectra in Fig. 6.5(b)). For detection the V-polarization output channel was used, and this output was aligned on a 75-cm grating spectrometer (PI Acton), equipped with a liquid-nitrogen cooled CCD camera. As compared to PL readout that used back scattering into the singe-mode fiber (Fig.5.5), the data quality shows a great improvement. It shows several features of sub-band-gap emission by low-doped n-GaAs: emission by free excitons, neutral donor-bound excitons, ionized donor-bound excitons, acceptor-bound excitons, as well as the so-called two-electron satellites (TES) [6, 7] of the neutral donor-bound excitons (transitions from D^0X levels to an excited state of the D^0 system, which has the electron in a $2s$ or $2p$ orbital of the envelope wave function, see also Chapter 1).

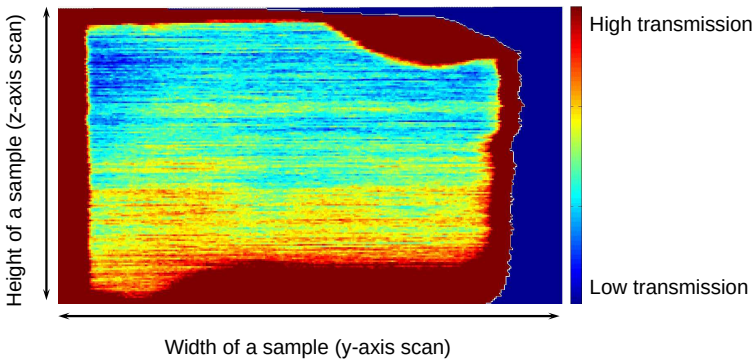

Figure 6.6: Result of imaging a ∼1.5 by ∼2.5 mm^2 n-GaAs sample via the free-exciton response, measured in transmission. The image is built via two-dimensional scanning of the sample position with the x- and z-direction piezo motors (directions as defined in Fig. 5.1). The experiment used a single excitation laser, with the wavelength fixed in the transmission window between the $X_{n=1}$ and $X_{n=2}$ free-exciton absorption resonances (see also Fig. 3.2(a)). The results reflect both the sample geometry and small changes in the transmission due to position-dependent shifts of the bang gap and excitonic transitions (which provides a signal for strain in the material). The resolution of this image is limited by the minimum spot-size in the focus of the setup (∼2 μm diameter).

6.3.4 Imaging tests on n-GaAs sample

Our approach to studying thin n-GaAs layers is based on transferring them onto a sapphire substrate (Chapter 2, 5). This process may result in local strain at

a few places in such a n-GaAs layer. The presence of strain causes shifts in the GaAs band gap, and shifts and splittings of spectral lines of excitonic transitions [8, 9, 10]. Thus, while scanning the sample position with respect to the focus of the laser beam, and with the laser at a fixed wavelength near an excitonic transition, transmission studies of the material can give an imaging signal that reflects local strain. We apply this approach by applying a single laser that is fixed at a wavelength between the free-exciton $X_{n=1}$ and $X_{n=2}$ absorption resonances, with the sample at 4.2 K and in zero magnetic field (see Fig. 3.2(a)). For having a strong response to the occurrence of strain (which shifts the free exciton lines [9, 10]) the laser is tuned to a steep part in the absorption spectrum, at the edge of the $X_{n=2}$ transition. Next, we use the piezo-motor stage for scanning the sample position with respect to the laser focus. Results of sample transmission as a function of position in the sample, obtained in this manner, are presented in Fig. 6.6. After obtaining this data, spectroscopy as a function of laser frequency is performed on a region of well-defined transmission, such that the transmission information can be turned into information about the local spectral shift for the material.

This imaging method saves a lot of time in finding a suitable spot on a $\sim$2 by $\sim$2 mm^2 GaAs layer: for our research we need areas that have homogeneous strain properties (to avoid inhomogeneous broadening of optical transitions), for laser beams that are typically tuned to give 2 to 50 μm spot diameters on the sample. In addition, it is desirable to select areas with either no significant strain, or strain that is high enough to cause significant shifts and splittings of spectral lines [8]. Further application of this approach is reported in Ref. [2].

6.4 Summary and outlook

This chapter presented further development of the cryogenic microscope that has been central for obtaining the results in this thesis. While the performance of the new part (polarization-selective output from the measurement volume) is not ideal, it clearly improved the experimental setup. Besides use for the tests presented in this chapter this instrument has recently been essential for a range of GaAs D^0 studies in our team [1, 2, 3]. In addition, it realizes a significant instrumentation step for experiments that make further use (beyond only direct detection) of quantum-optical light pulses that have been emitted by a material system in the sample volume.

Acknowledgements

We thank B. H. J. Wolfs for help and acknowledge the Dutch Foundation for Fundamental Research on Matter (FOM), the Netherlands Organization for Scientific Research (NWO), and the German programs DFG-SFB 491 and BMBF-nanoQUIT for funding.

References

[1] A. R. Onur, *Optical control of mesoscopic spin ensembles in gallium arsenide* (PhD thesis, University of Groningen, 2015).

[2] J. P. de Jong, *Optically addressing semiconductor electron-spin ensembles with tunable nuclear-spin environments* (PhD thesis, University of Groningen, 2016).

[3] A. R. Onur, J. P. de Jong, D. O'Shea, D. Reuter, A. D. Wieck, and C. H. van der Wal, *Stabilizing nuclear spins around semiconductor electrons via the interplay of optical coherent population trapping and dynamic nuclear polarization*, Phys. Rev. B **93**, 161204(R) (2016).

[4] Maksym Sladkov, M. P. Bakker, A. U. Chaubal, D. Reuter, A. D. Wieck, and C. H. van der Wal, *Polarization-preserving confocal microscope for optical experiments in a dilution refrigerator with high magnetic field*, Rev. Sci. Instr. **82**, 023709 (2011).

[5] Purchased and data sheet from Schäfter und Kirchhoff (Germany), (http://www.sukhamburg.de).

[6] V. A. Karasyuk, D. G. S. Beckett, M. K. Nissen, A. Villemaire, T. W. Steiner, and M. L. W. Thewalt, *Fourier-transform magnetophotoluminescence spectroscopy of donor-bound excitons in GaAs*, Phys. Rev. B **49**, 16381 (1994).

[7] K.-M. C. Fu, *Optical Manipulation of Electron Spins Bound to Neutral Donors in GaAs* (PhD thesis, Stanford University, 2007).

[8] V. A. Karasyuk, M. L. W. Thewalt, and A. J. SpringThorpe, *Strain effects on bound exciton luminescence in epitaxial GaAs studied using a wafer bending technique*, Phys. Stat. Sol. B **210**, 353 (1998).

[9] W. Schairer, D. Bimberg, W. Kottler, K. Cho, and M. Schmidt, *Piezospec- troscopic and magneto-optical study of the Sn-acceptor in GaAs*, Phys. Rev. B **13**, 3452 (1976).

[10] D. C. Reynolds, C. W. Litton, T. C. Collins, and S. B. Nam, *Free-exciton energy spectrum in GaAs*, Phys. Rev. B **13**, 761 (1976).